THE DESIGN OF TRANSONIC AIRFOILS UNDER CONSIDERATION OF SHOCK WAVE BOUNDARY LAYER INTERACTION

H. Sobieczky and E. Stanewsky
DFVLR - AVA, Inst. f. Strömungsmechanik.
Göttingen, Germany.

Abstract

new indirect design method for inviscid two-ıensional compressible flow based on the ho-ɡraph transformation and used for the design shockfree airfoils was extended to include ak shocks and the displacement due to boun-·y layers with and without separation. Shock-ındary layer interaction measurements were ·ried out and the results of the theory were npared with the experiments. Measured boun-·y layer parameters were, in addition, com-·ed to boundary layer computations. It will be ›wn that the extended hodograph method com-ed with a boundary layer computation method well suited to design transonic flows including ›ck-boundary layer interaction.

Nomenclature

	chord
	lift coefficient
	pressure coefficient
ΓE	pressure coefficient at the trailing edge
	Machnumber (local)
	static pressure (local)
	variable of state (Machnumber function)
	Reynoldsnumber, $c \cdot V_\infty/\nu_\infty$
	airfoil thickness
	free stream velocity
	velocity nondimensionalized with critical speed
	local streamwise velocity components
	velocity at the edge of the boundary layer
	coordinates of the flow plane
$c)_s$	shock location
	angle of attack
	local shock angle
	boundary layer thickness
	displacement thickness
	momentum thickness
	variable of state (local flow angle)
ψ	flow potential and stream function
	complex rheograph plane
	density

›scripts

	freestream conditions
	stagnation conditions

›erscripts

	critical conditions
	ahead shock
	behind shock

Abbreviation

220 K, 15 L Identification of size and location of tripping devices (here: No. 220 Carborundum grit in 15 % chord).

1. INTRODUCTION

This paper consists of two parts. In the first part a hodograph method for the design of inviscid transonic airfoil flow is described. The method is applied at first to shockless flow, where the graphic and educating character of a modified hodograph is brought into connection with the design principles for desired types of supercritical airfoils. Then the method and its boundary- and initial value problems are extended to flow with shocks. It concentrates on physical boundaries, which qualitatively stem from the displacement of a turbulent boundary layer, interacting with a transonic recompression shock.

In the second part of the paper experiments in the transonic wind tunnel are described which were carried out to measure the structure of the boundary layer as well as the outer flow. The assumptions of the potential outer flow models, described in the first part, are thereby illustrated and supplied quantitatively.

2. POTENTIAL FLOW

2.1 The use of modified hodograph planes

For the following introduction of hodograph variables, we consider plane, compressible, inviscid flow.

As indipendent variable, the Mach number function

$$q(M) = \int_1^W \sqrt{|1-M^2|}\ \frac{dW}{W} \qquad (1)$$

is used, where W is the local speed, nondimensionalized with the critical speed. Another Mach number function is defined by

$$K(M) = K(q(M)) = \frac{\rho_o}{\rho(M)} \sqrt{|1-M^2|} \qquad (2)$$

A second independent variable is the local flow angle and in both of these variables of state, the basic equations of plane, compressible potential

flow become linear:

$$\Phi_q = \pm K \cdot \Psi_\vartheta, \qquad \Phi_\vartheta = K \cdot \Psi_q. \tag{3}$$

Φ is the potential, Ψ the streamfunction; the system is of elliptic type in the half plane $q < 0$ (negative sign in the first equation) which represents the state of subsonic flow, and of hyperbolic type in the half plane $q > 0$ (positive sign) representing supersonic flow, see Fig. 1. In the hyperbolic domain H, the characteristics as lines of 45° inclination are drawn. Both domains are connected along the sonic line $q = 0$.

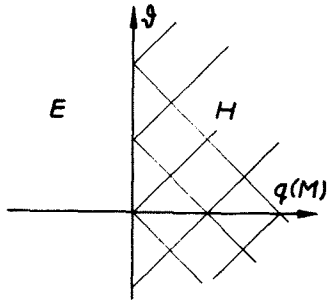

Figure 1. The plane of state

The basic equations, (3), form a system of generalized potentials which may be expanded into a Cauchy-Riemann-system ($q < 0$) or into the wave equation ($q > 0$) locally with $K = \text{const}$. Experience with these systems therefore may be used to study local solutions of (3). The basic system does not change its nature if the plane of state

$$\zeta_o = q + i\vartheta \tag{4}$$

is mapped conformally in the elliptic ($q \leq 0$) or mapped characteristically in the hyperbolic ($q \geq 0$) region. Such mappings are useful if boundary value problems are simplified by it. Subject of this paper are the boundary value problems of the potential outer flow of supercritical airfoil flow with or without a recompression shock, Fig. 2.

Figure 2. Supercritical airfoil flow.

We assume that the shocks are weak enough so that potential flow behind them still holds. For shockless flow the boundary value problem in ζ_o makes it useful to map the elliptic region conformally by the functions

$$\zeta_1 = e^{\zeta_o}, \tag{5}$$

$$\zeta_2 = (\zeta_1 - \zeta_{1N})^{1/2} \tag{6}$$

and solve the elliptic system in ζ_1 or rather ζ_2, Fig. 3

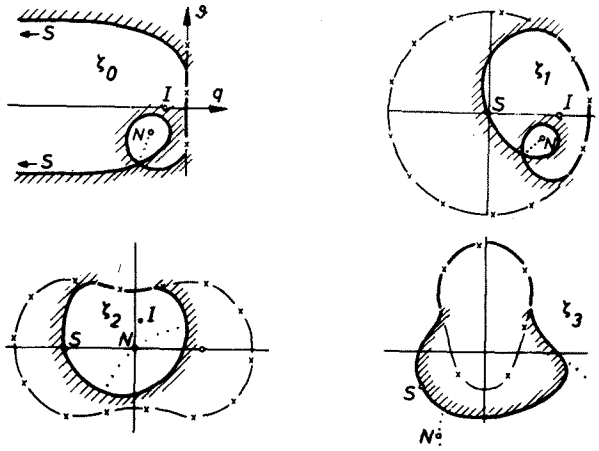

Figure 3. Conformal mapping of the elliptic region.

The plane ζ_1 no more excludes the state of a stagnation point S from the picture, ($q(M \to 0) \to -\infty$), while the plane ζ_2, in addition, removes the occurence of a second Riemann sheet with its branch point N. Furthermore (see Fig. 3) in the plane

$$\zeta_3 = (\zeta_2 - \zeta_{2I})^{-1} \tag{7}$$

the boundary value problem is quite similar to a problem given in the physical plane; the incompressible flow past an arbitrary body.

Thus, the mapping is introducing some analogy in formulating boundary value problems. In addition, the basic equation itself has a physical analogy, as will be described and used later in this paper. Therefore, the planes of state, ζ , are named "rheograph" planes, due to both their relationship and their difference to the hodograph plane.

2.2 Methods of solution in a rheograph plane

Before these basic remarks are applied to supercritical airfoils, a mixed boundary value problem will be formulated in a rheograph plane and methods of solution for the basic equations will be described.

Given is a region E in the plane $\zeta_o = q + i\vartheta$ (Fig. 4, left side). Its boundary in $q < 0$ is $\Psi = \Psi_o = \text{const}$ and along the sonic line, $q = 0$, it is the distribution $\Phi^*_\vartheta \cdot \Psi^{*-1} = F(\vartheta)$. The interior of E may include singularities. This elliptic problem is well posed; due to the linearity of the basic system it may be solved by several methods.

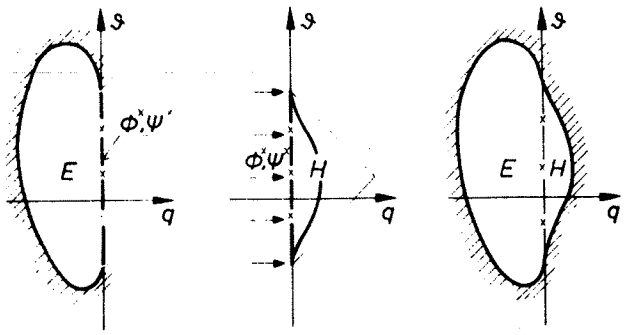

Figure 4. Transonic boundary value problem.

Now, with the solution $\Phi^*(\vartheta)$, $\Psi^*(\vartheta)$ along the sonic line an initial - value problem for the hyperbolic region H is formulated (Fig. 4 center) which means physically that the sonic line and the flow angle on it are given, while the supersonic field and a physical boundary contour in it are the solution. With the method of characteristics, Φ and Ψ in the triangle H are calculated now, as well as the curve $\Psi = \Psi_0$. Due to common values Φ^*, Ψ^* along the contacting sonic line, both parts of the solution may be taken as one solution of the system (3) (Fig. 4., right - hand side). Integration of potential and streamfunction results in the coordinates of the physical plane in the well known way.

For the development of numerical methods of solution of system (3), experience with particular solutions is of some use. The first author has investigated a class of homogene solutions of the near sonic expansion of (3), [1], which are related to the solutions given by Guderley, Frankl, Germain and other authors.

To solve the elliptic system (3) numerically either Φ or Ψ is eliminated. For the remaining Ψ or Φ a linear Poisson equation is obtained which may be treated successfully with the methods solving the Laplace equation.

The hyperbolic system (3), as already mentioned, is solved by methods of characteristics starting at the sonic line.

Eberle [2] calculates the solution of the elliptic system with a new panel method. It works in plane ζ_3, (7), so the method was developped from programs computing the incompressible flow past airfoils.

The first author uses the rheo-electrical analogy to solve the elliptic system (3). Electrostatic potential distributions in plane conductors of variing conductivity are evaluated. Simplicity of the set up and primarily the graphic and educating character of the analogy are main reasons of its application. The electrolytic tank as well as inhomogenized TELEDELTOS-paper is used and a small data acquisition system measures the potential distribution. Numerical evaluation, including calculation of the hyperbolic domain, drawing calcomp plots and punching airfoil coordinates, is taking 1 - 2 minutes on a IBM 370 - 158 computer.

2.3 Redesign of a given shockless airfoil

In this paper results are presented which have been calculated with help of the rheoelectrical analogy. Some analytically or numerically known examples were used to calibrate the analog setup in order to know about the degree of exactness of the results. One of these examples was the wellknown shockless lifting airfoil KORN 1, see [3]. As a first test, the analog flow was designed using perforated TELEDELTOS and the rheograph plane ζ_1, Fig. 5.

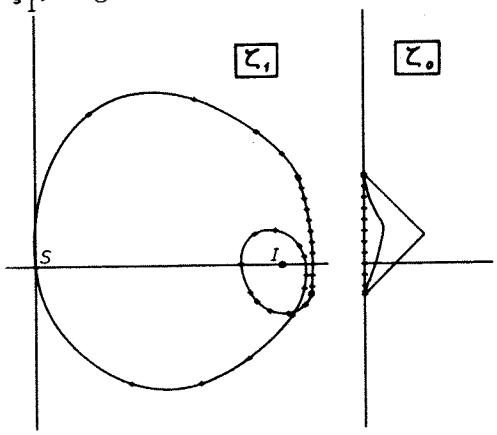

Figure 5. Rheograph ζ_1, ζ_0 of airfoil KORN 1.

Results were very satisfying, nevertheless there was another test using the plane ζ_2 for the analog flow which avoided the electrical coupling of the second Riemann sheet. The locally variing perforation was replaced by the use of compressed layers of TELEDELTOS-paper and the boundary along the sonic line was produced by a continuation of the elliptic type flow beyond the sonic line (see Fig. 6).

As mentioned earlier in this paper, for a rheograph ζ_2 the branchpoint in ζ_1 has to be known. In the case of this airfoil, this point is known from the original Garabedian - Korn design [4], using a complex extension of the characteristics method. The relationship between ζ_2 and the real part plane of this method is quite obvious.

In Fig. 6 some streamlines are drawn: they are measured as lines of constant electrical potential. Fig. 7 shows the analog set up principle.

A source of 12 V dc feeds the singularity I. The contour is painted with conducting silver and therefore on a constant value of electric potential. This is variied using a potentiometer R_c in order to bring the branch point of the contour potential into the mapped stagnation point S.

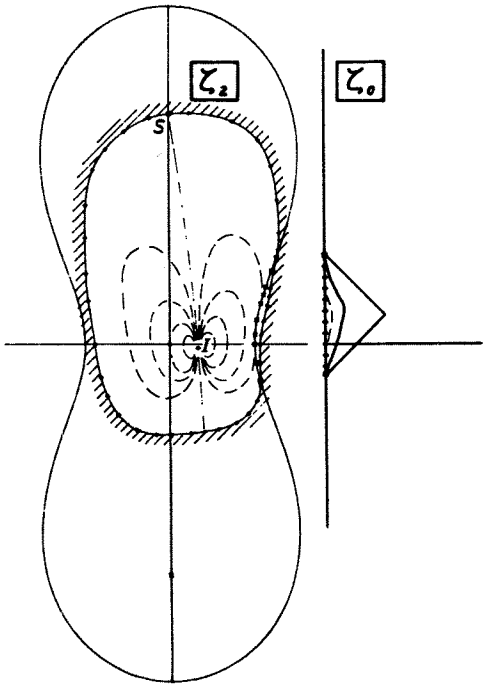

Figure 6. Rheograph ζ_2, ζ_0 of airfoil KORN 1.

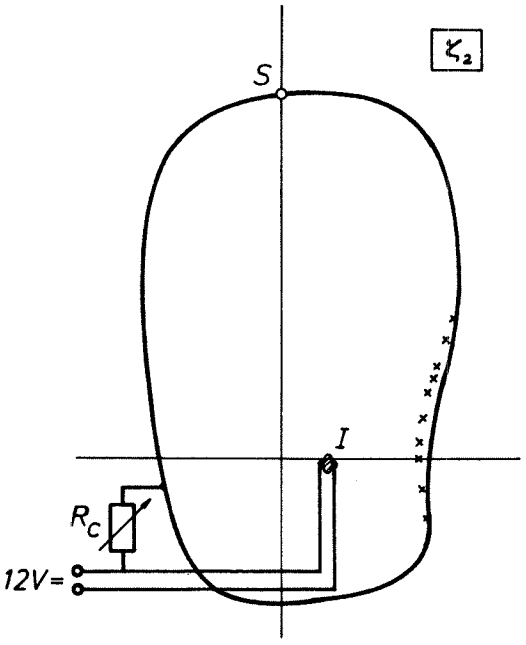

Figure 7. Analog flow setup.

Electric potential in the points along the sonic line and the prescribed analytical continuation beyond the sonic line are giving the initial data for the method of characteristics in the hyperbolic region of ζ_0 (Fig. 6, right hand side). The gradient of the electric potential along the elliptic boundary, finally now gives the data to integrate the flow potential along the airfoil contour.

The results of this redesign were compared with analysis results for the airfoil obtained (Fig. 8). Comparison shows the best agreement at a slightly different design point, $M_\infty = 0,753$, $\alpha = -0,1^\circ$, while it was intended to have $M_\infty = 0,75$, $\alpha = 0$. This has its reason in the imperfectness of the electrical singularity I (Fig. 7), which must be not to small. The effective singular point therefore lies in some (tolerable) distance of the geometrically intended one.

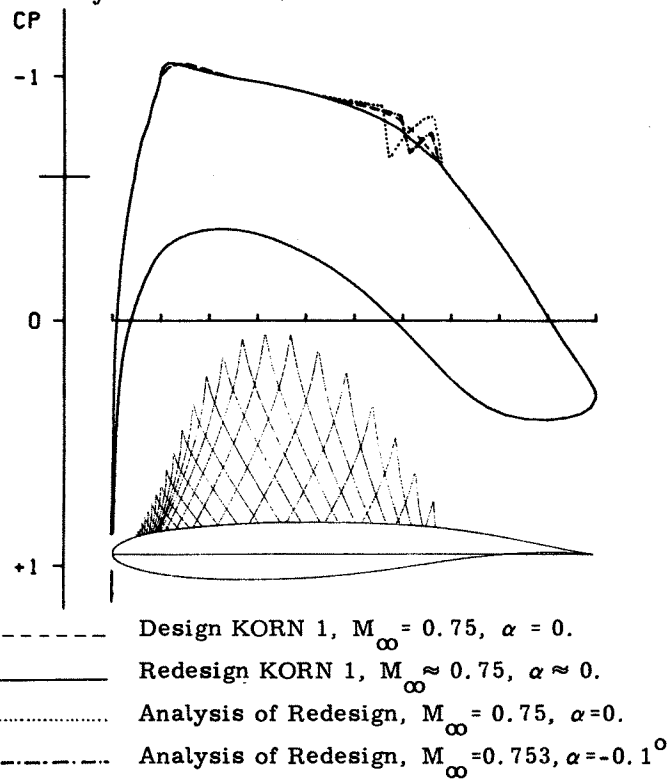

Figure 8. Redesign of airfoil KORN 1 and analysis.

2.4 Design of shockless potential outer flows.

The airfoil KORN 1 has been redesigned to obtain information about accuracy and effectiveness of this special design method making use of the rheoelectrical analogy, but also many analysis methods and wind tunnel tests made use of this airfoil , especially to study viscous effects both in computational and experimental approach. But just this well known airfoil was designed with a zero trailing edge thickness. So it is not possible to use it as a potential outer flow when taking into account viscous effects. Other designs allow such a subtraction of a boundary layer displacement. In the rheograph plane, thick trailing edges may be obtained by rotating the orientation of the dipol-singularity in I (see Figs. 6, 7).

Designing a contour in a rheograph plane means

designing a special hodograph contour at first. The designer is able to prescribe the type of pressure distribution on the resulting airfoil to a high degree,as is beeing illustrated inFigs. 9 and 10.

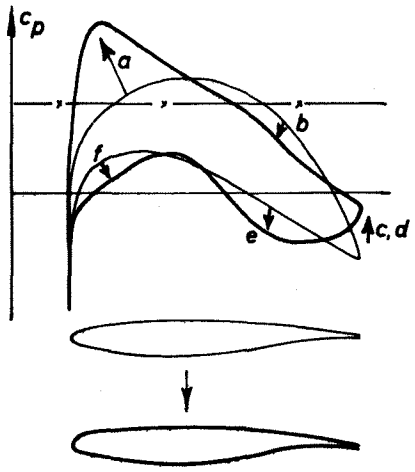

Figure 9. Optimizing a shockless design.

To show this in a short way, an existing shockless design is taken (Fig. 9, thin lines for airfoil and pressure distribution). This airfoil should be optimized now in the sense of higher lift and better avoidance of high positive pressure gradient at the trailing edge. In Fig. 9, arrows 'a - f' show a desireable change of the pressure distribution: Arrow 'a' creates a "peaky" pressure distribution, while a more gradual pressure rise is achieved by 'b', 'c' and 'd', with lowering pressure at the trailing edge. A "rear loading" is obtained by 'e', finally 'f' brings more lift at the leading edge region and with 'a' a better c_m is the result.

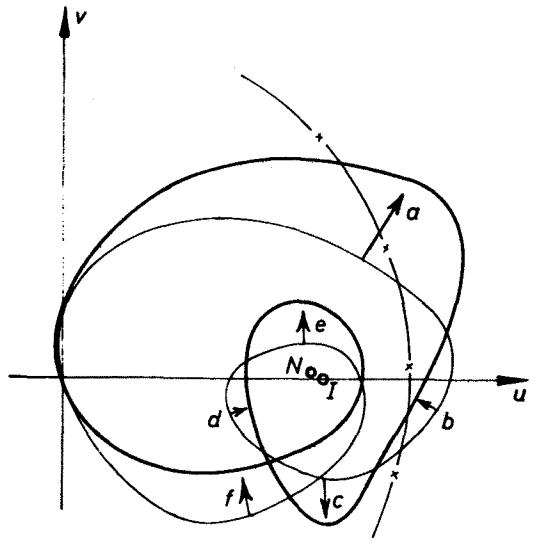

Figure 10. Hodograph of shockless designs.

In Fig. 10, the changes 'a - f' of the initial design hodograph are drawn qualitively. Lifting the whole hodograph region near the sonic circle, ('a','b'), creates the "peaky" type pressure distribution and slow pressure rise in the recompression area. This type is relatively insensitive to changes of the design conditions, a well known fact. The deformation 'c' should be at the trailing edge image, Garabedian [5] proposes even a corner, directing towards the sonic circle. In the complex characteristics method this is obtained by a saddlepoint of higher order; the designed trailing edge has a singular curvature locally.

Arrows 'd, e' deform the second sheet of the hodograph. Rear loading of the airfoil is mostly influenced by the geometry of this second sheet. Arrow 'f' deforms the hodograph near the origin S. Of course, every hodograph with a stagnation point has to go through this origin.

This brief sketch of typical design parameters should illustrate the importance of some graphical tool for the designer. The most effective, presently working hodograph methods which are the already mentioned Garabedian - Korn method and the Nieuwland - Boerstoel method [6] use higher order regular solutions of the hodograph equations for deformations of the design hodograph. Eberle's panel method or the use of an electric analog flow allows the graphical choice of a boundary. In any hodograph method the relative situation of the free stream singularity I and the branchpoint N has to be variied in order to obtain correctly closed trailing edges of a desired thickness.

These given illustrations can only give an idea, in which way systematic design could be carried out. In a small frame, the first author has performed the design of series of potential outer flows, forming families of continual change. Such series are a basis for numerical optimization procedures like the method by Hicks, Murman and Vanderplaats [7].

Fig. 11 shows two airfoils of a design series with variing peak at the pressure distribution. Boundary layer displacement was subtracted from the potential outer flow, it was claculated with the Nash-Macdonald method with a Reynolds number Re = 10^7. Wind tunnel tests with one of the more peaky type airfoils of this family are presently carried out, further tests will be used to study trailing edge interference on a relatively blunt trailing edge.

$M_\infty = 0.73$
$Re = 10^7$.

A: $c_L = 0.53$
$t/c = 0.132$

B: $c_L = 0.55$
$t/c = 0.135$

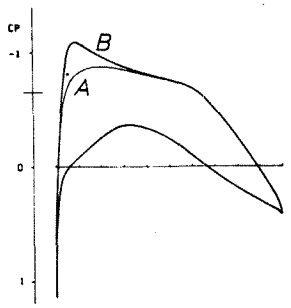

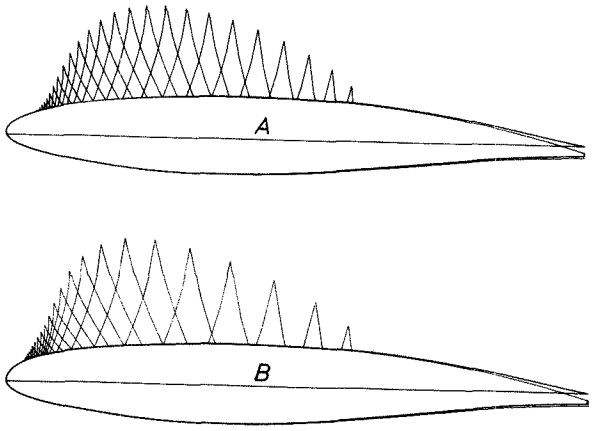

Figure 11. Two shockless airfoil designs.

2.5 Isentropic recompression shock models.

In the following remarks the basis of design will be extended in order to include recompression shocks in the flow field. This does not mean, that an airfoil flow should not be shockless in its design conditions, if this seems possible. Boerstoel (8) presents limits in Mach number, lift and thickness, beyond which no shockless flow is presently known. When trying to obtain a shockless airfoil with the present method in the region beyond those given limits, one would usually get a flow with limit lines in the supersonic region which is physically impossible.

It seems useful therefore at least in principle, to know the mapping of a flow with shocks into the rheograph plane, the design plane. It is assumed here that the shocks to be designed will be weak enough that potential flow behind the shock is still existing. For the design of weak shocks therefore the transonic expansion of the shock relations may be used. It describes the connection between the velocity vectors ahead of and behind an oblique shockwave, Fig. 12.

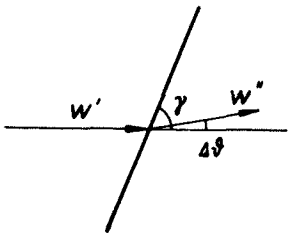

Figure 12. Oblique shockwave.

In the hodograph plane and therefore also in the introduced rheograph planes ζ, the shock relations are represented by the shockpolars, which will be used now to solve a special design problem:

An element of transonic potential flow with $M < 1$ and its mapping into ζ_o is given. In Fig. 13 this is illustrated by some streamlines Ψ = const. in the half plane $q < 0$. These streamlines are intersected by a given curve A"B". On the curve the solution of the elliptic system (3) gives a distribution of $\Phi = \Phi''(q''), \Psi = \Psi''(q'')$.

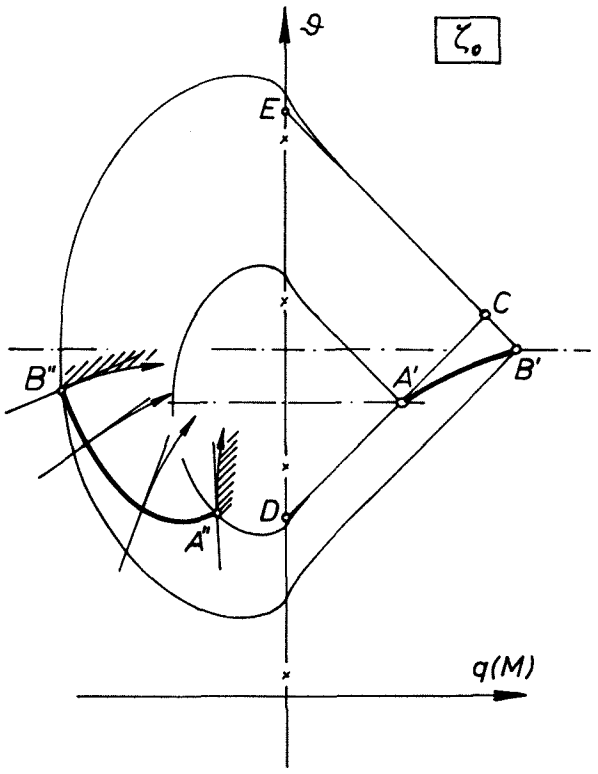

Figure 13. Transonic shock design.

It is postulated now that curve A"B" is the mapping of a shock backside. The mapping of the shock front in the supersonic region $q > 0$ is to be found. For this, the shockpolar and its relation to the shock inclination is needed. The intersection angle between curve A"B" and the emanating streamlines gives the shock inclination and with the local value of q(M) the shockpolar in any point of A"B" can be found. Shock polars in the limiting points A", B" are drawn; with them the limits of the shock front mapping curve A'B' are given. Along A'B' there is the corresponding distribution $\Phi = \Phi'(q') = \Phi''(q'')$, $\Psi = \Psi'(q') = \Psi''(q'')$ since no jump in streamfunction and potential across the shock is allowed. This distribution now has to be fitted with a solution of the hyperbolic system (3). With given data Φ^*, Ψ^* along the sonic line between the points D and E as part of the boundary of the previously

solved elliptic problem, the triangle DEC is calculated with the method of characteristics. With the solutions along A'C and A'B', the same method solves field A'B'C.

With this principle, a shockwave of given strength can be designed. Special attention has to be drawn to the ending points of the shock in the flowfield and on the contour.

In the flowfield with a local supersonic region, as already wellknown, a recompression shock forms by gradual coalescence of compression characteristics, see Fig. 14.

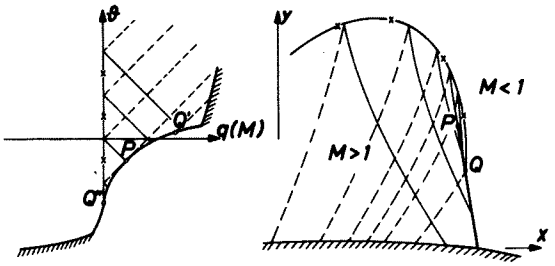

Figure 14. Shock formation in free flow.

This figure shows also the mapping of both sides of the shock. In point P they are connected, with shock strength approaching zero.

More complicated is the structure of the flowfield, the shock and the mapping into the hodograph plane of the footpoint region on a convex contour for inviscid flow. The local solution with a logarithmic singularity, given by Oswatitsch and Zierep [9], brings a saddle point R of the Mach number distribution (Fig. 15) which mappes into a branch point with a relatively small second Riemann's sheet.

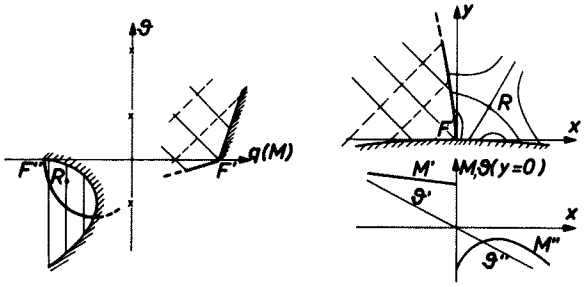

Figure 15. Shock ending on a curved wall.

An analytic treatment of the flows, sketched in Figs. 14 and 15, is given by the first author in [3].

In the case of including viscous effects, the curved wall boundary has to be modified in some manner to regard the displacement of the boundary layer. The wellknown experiments of Ackeret, Feldmann and Rott [10] gave a first idea about the thickening of laminar and turbulent boundary layers, when passing through a shock. From these and other tests, an idealized model of wall contour may be derived, which is treated analytically by the first author in [11] and regards turbulent shock-boundary layer interaction in a simplified way (Fig. 16).

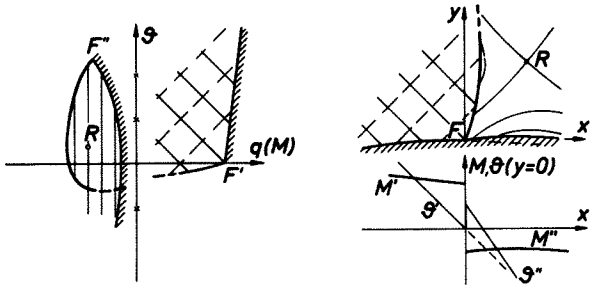

Figure 16. Shock formation at viscous ramp model.

At the right side of Fig. 16 in the flow plane x,y an undisturbed supersonic flow past a convex wall contour meets a ramp of certain angle in the point F. The convex contour is continued with higher curvature downstream of F. If the ramp angle does not lead to a detached shock wave, there will be an oblique shock formation in F. With use of the shock polar, the "strong shock" solution gives the pressure (Mach number -) jump and together with the shock inclination formula , the flow field as well as the local shock geometry may be described by a series expansion of local solutions of the elliptic basic equations (3). At the footpoint F, the shock is forming into a downstream direction, but is bent upstream in the field. Thus the oblique shock on the contour becomes normal at some point in the flow field, where it meets the incoming shock (Fig. 14).

At the left side of Fig. 16 the mapping into the rheograph plane ζ_0 is drawn. Like the normal shock flow model, also this flow maps into a second Riemann's sheet due to the occurrence of a saddlepoint R of the Mach number distribution in the flow field. A prescribed elliptic boundary detail in ζ_0 of generally this type, imbedded into boundaries of supercritical airfoil flow described in the previous chapters, allows the design of potential flows past airfoils with dicontinuities of the local flow angle which may be interpreted as prescribed shock - boundary layer interaction without or even with separation.

Before the viscous ramp model may be used fruitfully for this purpose, experience with results of viscous interaction measurements as well as with boundary layer computation methods has to be gained.

3. EXPERIMENTAL RESULTS ON TRANSONIC SHOCK-BOUNDARY LAYER INTERACTION

Boundary layer measurements on a supercritical airfoil were carried out for two reasons: to study the flow development that leads to large transonic scale effects and to obtain experimental results in support of the theoretical work outlined in the preceding chapters.

3.1 Test set-up and test conditions

The investigation was conducted in the 1x1 Meter Transonic Wind Tunnel of the DFVLR-AVA Göttingen using a supercritical airfoil designed by the DORNIER GmbH[12]. The wind tunnel is a continuous closed circuit tunnel whose test section consists of four perforated walls with holes slanted 30° to the flow direction. The open area ratio of the walls is 6% [13].

The model and boundary layer probe installation and the contour of the airfoil investigated here are shown in Fig. 17.

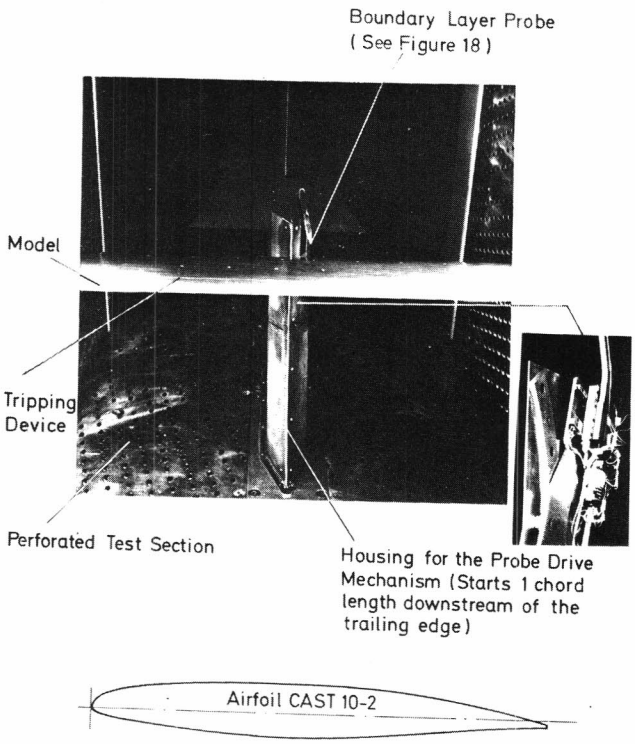

Figure 17. Model and model installation.

The model had a span of b = 1000 mm and a chord of c = 200 mm resulting in span/chord and tunnel-height/chord ratios of 5. Since the main objective of the present tests was to determine the overall boundary layer development on a certain type of supercritical airfoil - as it is affected by the interaction with the shock and the subsequent adverse pressure gradient - and flow quantities in the outer field, the use of a conventional boundary layer probe was deemed sufficient. The probe, consisting of a 0.15 mm high Pitot probe, a static probe and a probe to measure flow angularity, is shown in Fig. 18.

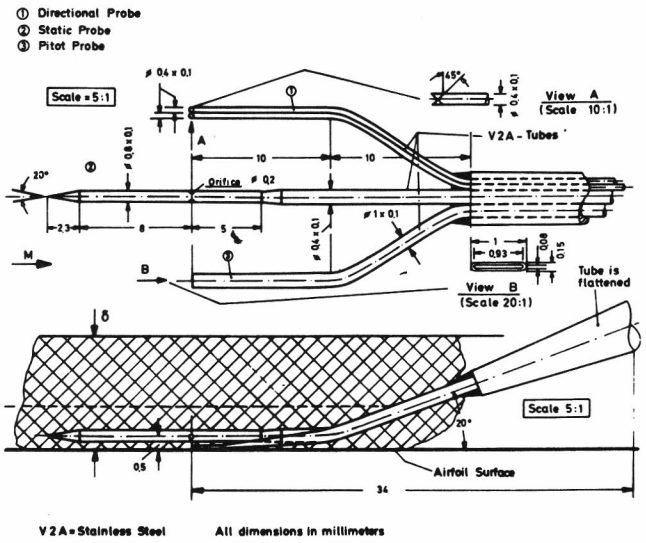

Figure 18. Boundary layer probe.

The freestream conditions for which boundary layer measurement were carried out up to now are summarized in Table 1. In the context of the present paper we will, however, only consider the case $M_\infty = 0.771$, $\alpha = 1.1°$.

Table 1. Test conditions

M_∞	α °	$\alpha_{geom.}$ °	Transition
0.761	1.14	2.0	Free
0.761	1.14	2.0	220 K, 15 L +
0.761	3.49	4.5	Free
0.761	3.49	4.5	220 K, 15 L
0.771	1.10	2.0	Free
0.771	1.10	2.0	220 K, 15 L

Re = $2.4 \cdot 10^6$ + See Nomenclature

3.2 Experimental results

The investigation of a number of supercritical airfoils in the 1x1 Meter Transonic Tunnel of the DFVLR-AVA Göttingen has shown that the flow development on these airfoils may strongly be affected by the Reynolds number and the size and location of tripping devices attached to the model surface [12,14]. This is demonstrated in Fig. 19 where characteristic aerodynamic parameters for the airfoil CAST 10-2 are plotted as function of the Reynolds number and the tripping device location - it also becomes obvious from the upper surface pressure distributions presented later. The behavior of these parameters can be explained as follows: Increasing the Reynolds number or moving the tripping device upstream results in a forward movement of the transition

point which, in turn, causes an increase in the initial boundary layer thickness, i.e., the boundary layer thickness upstream of the shock on the upper surface of the airfoil. The interaction of the shock and the subsequent adverse pressure gradient with the increasingly thicker boundary layer results in drastic changes in the flow conditions in the vicinity of the trailing edge and hence in trailing edge pressure, shock location and lift coefficient (Fig. 19).

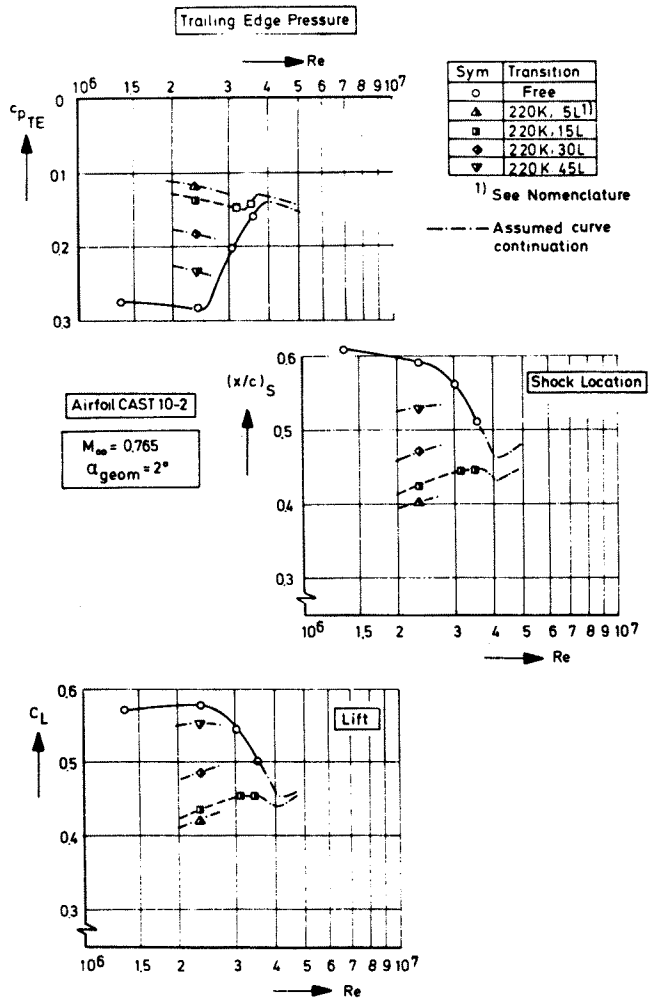

Figure 19. Effect of Reynolds number and trip location on characteristic aerodynamic parameters. Airfoil CAST 10-2. $M_\infty = 0.765$, $\alpha_{geom} = 2.0^\circ$.

Boundary layer and flow field measurements were carried out at various freestream conditions to study the effect of the shock and the subsequent adverse pressure gradient on the boundary layer development and to verify the conclusions drawn above which were solely based on surface pressure distributions. Within the context of the present paper, however, only data obtained for one of the test conditions will be considered. These data will also be used in conjunction with the potential flow model outlined in Chapter 2.

Fig. 20 shows measured surface pressure distributions and displacement thicknesses for the airfoil CAST 10-2 at freestream conditions (M_∞=0.771, α = 1.1°) above the design point - but still within the linear range of the lift curves - and free and forced transition.

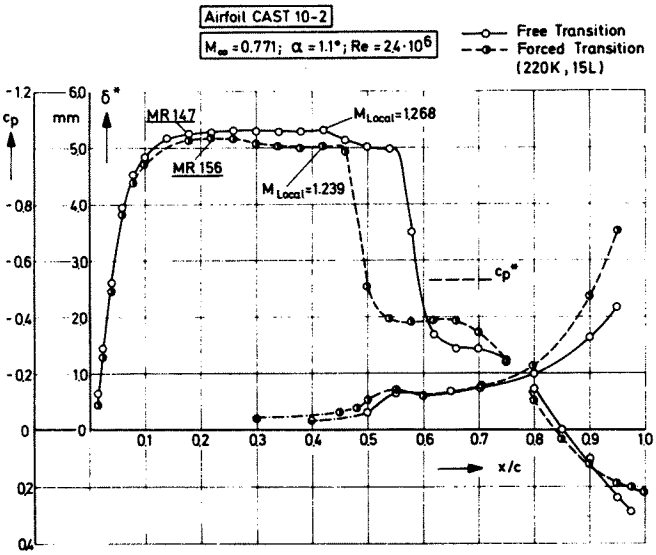

Figure 20. Comparison of surface pressure distributions and displacement thicknesses. Airfoil CAST 10-2. $M_\infty = 0.771$, $\alpha = 1.1^\circ$.

Considering first the data for forced transition, i.e., a turbulent boundary layer upstream of the shock, one sees that a gradual increase in displacement thickness occurs up to the point where the influence of the shock is first felt. Downstream of this point, the displacement thickness grows more rapidly due to the shock impinging on the boundary layer; a first maximum is reached at x/c = 0.55, i.e., just downstream of the pressure rise. In the range of the subsequent plateau in the pressure distribution, the displacement thickness decreases slightly, however, at x/c = 0.7 a renewed rapid increase commences due to the strong rear adverse pressure gradient which is a characteristic of this type of supercritical airfoil.

The boundary layer (Mach number) profiles measured with forced transition are shown in Fig. 21a. The fullness of the profiles decreases noticeably due to the influence of the shock (x/c=0.40 to 0.55) and an inflection point first becomes apparent at x/c = 0.55, the chord station of the first maximum in the displacement thickness. However, the boundary layer does not separate

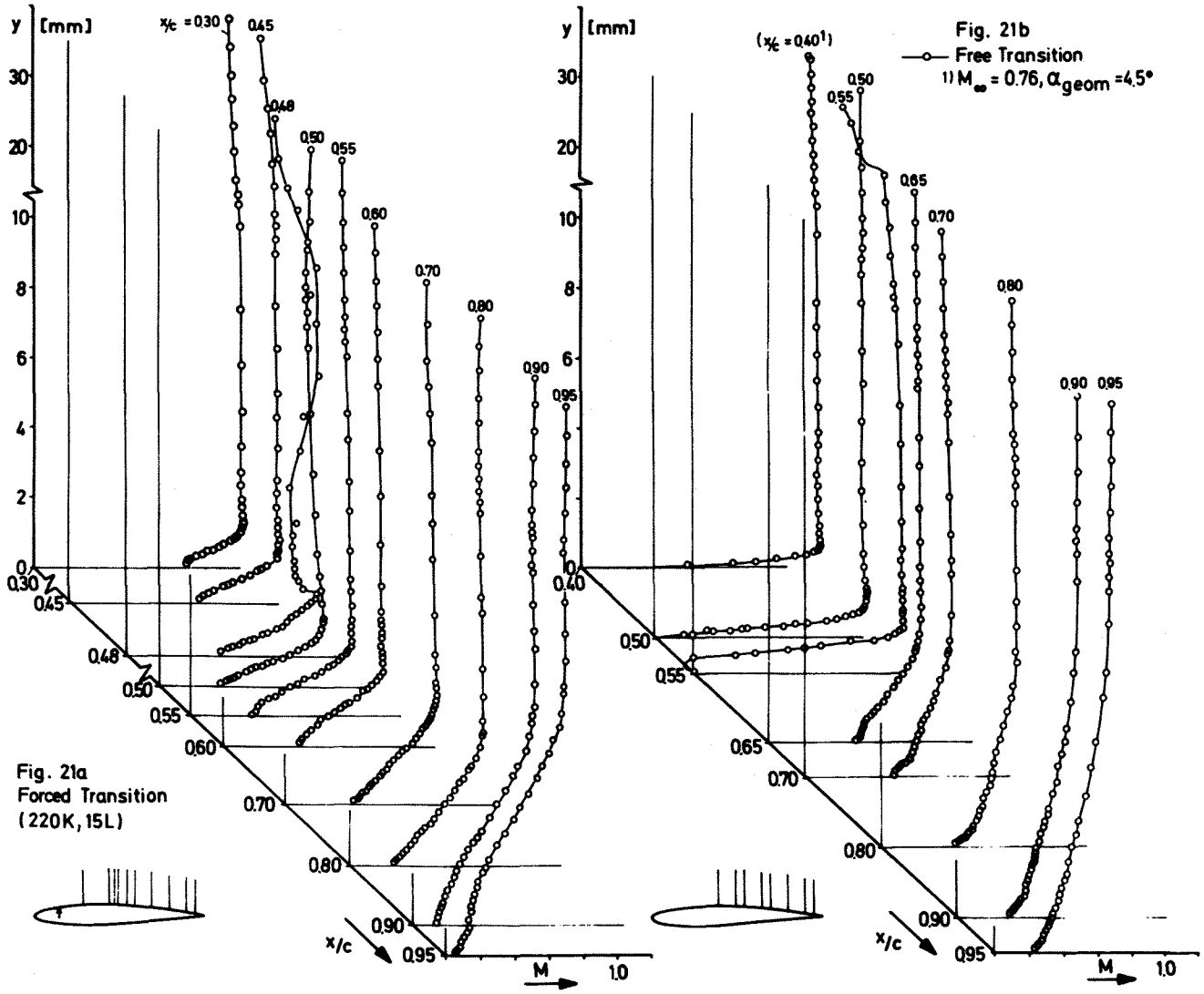

Figure 21. Boundary layer profiles and Mach number distribution in the field for free and forced transition. Airfoil CAST 10-2. $M_\infty = 0.771$, $\alpha = 1.1^\circ$.

at the shock. A relaxation of the boundary layer profiles takes place in the range of the pressure plateau downstream of the shock. At $x/c \geq 0.70$ a rapid deterioration of the boundary layer profiles commences due to the strong rear adverse pressure gradients and separation first occurs at $x/c = 0.95$. The boundary layer here reaches a thickness of about 4% of the chord ($\delta^*/c \approx 1.75\%$).

The pressure distribution in the case of free transition (Fig. 20) shows a slight increase in pressure upstream of the point where the main pressure rise due to shock occurs. In this range the displacement thickness increases steeply, reaching a plateau at about $x/c = 0.55$. The Mach number profiles in Fig. 21b indicate that the boundary layer approaching the shock is laminar. At $x/c = 0.55$, i.e., the beginning of the plateau in the displacement thickness, the laminar boundary layer has separated. Reattachment occurs somewhere between $x/c = 0.55$ and $x/c = 0.65$. Transition must also have taken place in this region since the boundary layer profile at $x/c = 0.65$ shows definitely turbulent characteristics. The now turbulent boundary layer relaxes up to a chord station of about $x/c = 0.70$. Downstream of this point, the rear adverse pressure gradient causes, as in the case of forced transition, a deterioration of the boundary layer profiles, however, the flow is, contrary to the development for forced transition, still far from separating. This is also indicated in Fig. 22 where the skin friction coefficients for the two cases considered here are compared.

A comparison of corresponding boundary layer profiles (Fig. 21) shows that in the range downstream of the shock the initially laminar boundary layer always exhibits fuller profiles than the boundary layer for which transition was forced at 15% chord. This, of course, results in the smaller displacement thickness over the rear of the airfoil (Fig. 20) and, as a consequence, in a smaller change of the effective airfoil contour and the flow conditions at the trailing edge.

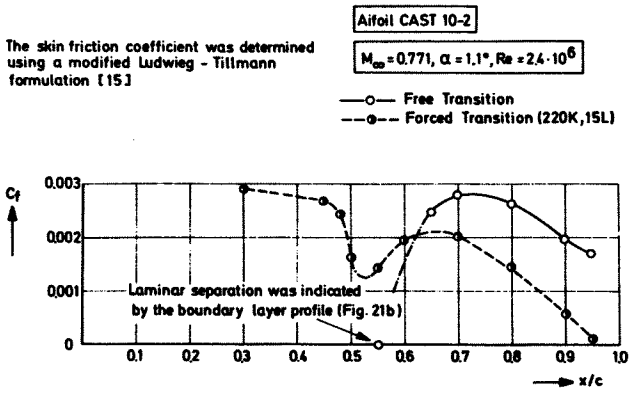

Figure 22. Comparison of skin friction coefficients. Airfoil CAST 10-2. $M_\infty = 0.771$, $\alpha = 1.1^\circ$.

This then explains the behavior of the characteristic aerodynamic parameters in Fig. 19, at least for the two extreme cases - free transition and a tripping device relatively far forward - considered here. Further boundary layer measurements will be carried out covering other test conditions of Fig. 19, such as, for instance, a higher Reynolds number and a tripping device location of 45 % chord.

Before proceeding to the next chapter, it seems appropriate to briefly consider the turbulent boundary layer profile and Mach number distribution in the flow field at x/c = 0.48 (Fig. 21a), corresponding to a point immediately downstream of the shock impingement. This distribution, which changes several times from subsonic to supersonic flow and back, indicates two things: Firstly, there must be a small local supersonic region downstream of the shock in the vicinity of the edge of the boundary layer and secondly, the shock wave must be curved being normal only at one point in the field (also see Fig. 16). A more detailed analysis of the flow field in the vicinity of the shock will be given in the next chapter.

3.3 Analysis of the potential outer flow.

The test case with forced transition (Figs. 20, 21a) was used for an analysis of the flow field in the vicinity of shock-boundary layer interaction with help of the previously mentioned shock models. The purpose of these calculations is to demonstrate, that potential outer flow reacts to the actual, viscous interaction quantitatively in the same way, as it does react to an idealized, inviscid interaction model.

Using the measurement Fig. 21a now, an exact location of the shockformation was assumed at $(x/c)_s = 0.475$. At this point the solution [11] of the subsonic flow behind the shock was applied, trying to fit the local surface Mach number as well as the viscous ramp geometry into the measured values of Fig. 20 in an optimal way. The result is drawn in Fig. 23.

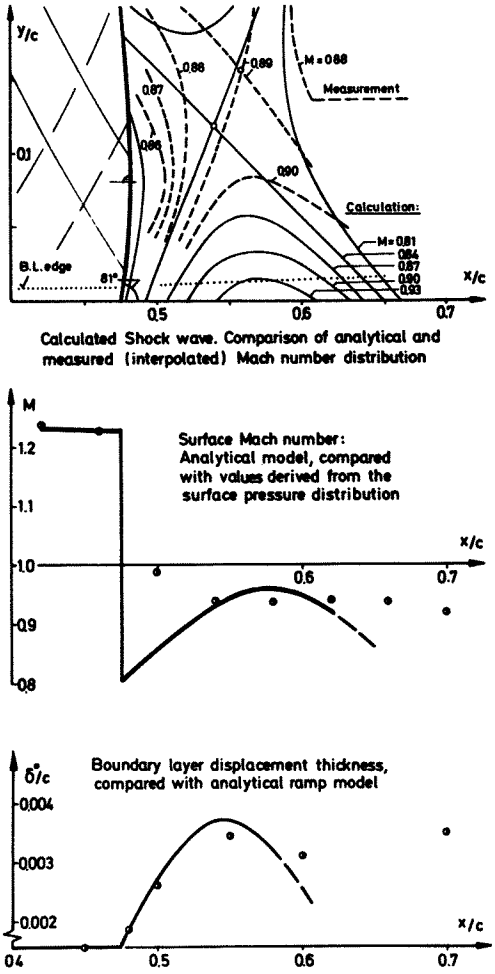

Figure 23. Shock - boundary layer interaction model on airfoil CAST 10-2 with forced transition.

In Fig. 23 above, the characteristics ahead of the shock and lines of constant Mach number are drawn. The Mach number distribution behind the shock is compared with interpolated values from the measurement (Fig. 21a). There is, at least qualitatively, a satisfying agreement between the analytical and the measured values: both distributions show the saddlepoint mentioned in the previous chapter.

In the center, the measured Mach number distribution is compared with the fitted analytical result. Like the inviscid flow model (Fig. 15), this solution exhibits a flow acceleration behind the shock, but not a logarithmically singular one.

Finally, the lower diagram compares the measured increase of the displacement thickness with the calculated local contour. A viscous ramp angle of 2.8^{o} fits well into the measured displacement thickness at $x/c = 0.475$, the local solution allows the analytical description of the viscous ramp, but the used first order solution of course gives agreement with the displacement thickness only in a vicinity of the shock footpoint, here for about 10 % of chord.

These illustrated quantitative studies of the application of a theoretical shock-boundary layer model are an important step toward the design of an assumed potential outer flow past an airfoil. In the present case, it was tried to design the supersonic part of the tested airfoil flow with forced transition. The result is shown in Fig. 24, together with the plane of state, the rheograph ζ_o. Illustration of several points should ease the understanding of the local flow behavior and the related boundary- and initial value problem to the reader.

At first, the airfoil geometry with a correcture due to boundary layer displacement and the given pressure distribution along AEF allows the mapping into ζ_o and the calculation of the supersonic region AEFDA by the method of characteristics, starting on the surface and terminating on a part AD of the sonic line, which is provided now with data Φ^*, Ψ^* (compare Fig. 4). If calculation of the complete supersonic field is required, as for this example, initial values Φ^*, Ψ^* are needed on the larger interval AB. Therefore the given distribution along AD has to be extended in a suitable way and the method of characteristics calculates now into the opposite direction towards the airfoil. Iteratively it took 4 corrections of Φ^*, Ψ^* along DB to gain the given complete contour mapping AEF.

Furthermore, the solution gives the rest of the local supersonic field, where coalescing compression characteristics (point P) indicate a shock formation. Both ends (P, F) of the shock curve, together with their local inclination are known now. In addition, curvature in F is approximately given by the local solution. A smoothly curved connection is assumed now, which cuts away a part of the supersonic field. Point G indicates the normal shock; in point Q the shock jump leads to sonic conditions. Shock formation in P occurs at a local Mach number $M \sim 1.04$. The expansion characteristic Q" E divides the supersonic region in two parts, connected with the subsonic field via the sonic line or the shock, respectively.

Using the local solution Fig. 23 as a guide, the exact isentropic shock polar now gives the mapping of the subsonic flow boundaries behind the shock, taking into account the measured boundary layer displacement thickening behind the shock. With airfoil geometry, boundary layer displacement and the pressure distribution along the whole

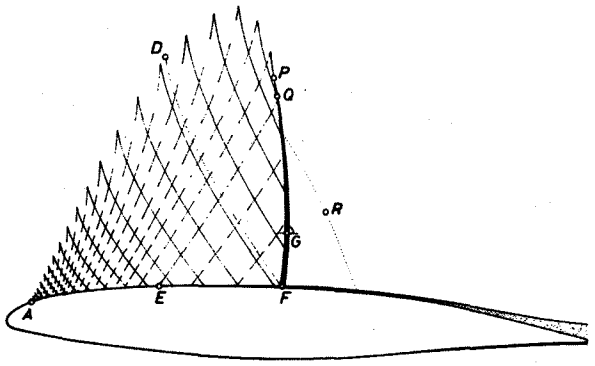

Figure 24a

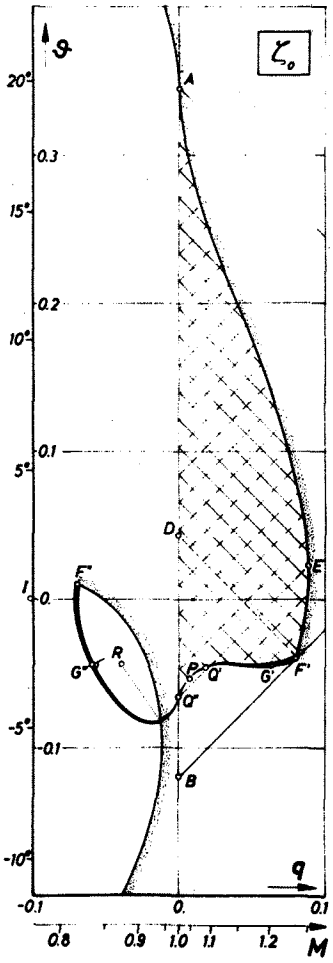

Figure 24b

Figure 24. Airfoil CAST 10-2: Local supersonic field, recompression shock and boundary layer displacement. Wind tunnel test with forced transition.
a. Physical plane
b. Rheograph plane ζ_o

airfoil contour in the subsonic field, the elliptic problem (though not to be solved here) is well posed now. A large part of the shock backside falls into the mentioned second Riemann's sheet of ζ_o, which is connected with the main sheet along the pointed line.

It looks, that mentioning a second sheet here rather discriminates a hodograph method as a design tool instead of showing its advantages, but

a purpose of this paper is to show the principal nature of potential outer flows with shocks, illustrated with some realistic data.

The branchpoint R in ζ_0 (saddle-point of Mach number distribution in the flow) is situated relatively close to the freestream singularity I, corresponding to the windtunnel test Mach number $M_\infty = 0.771$. This gives an idea, that the solution of the complete elliptic boundary is strongly affected by the situation of R and the geometry of the second sheet boundary.

Some conclusions may be drawn now from this illustrated combination of a recompression shock, viscous layer displacement and a hodograph method.

Firstly, hodograph methods are mostly useful to design flows without shocks; weak enough shocks in off design conditions are to be achieved mainly by the hodograph boundary choice (Fig. 10).

Secondly, the introduction of recompession shocks into the hodograph boundaries extends the design method with some relatively difficult, but well defined details in the posed problem.

Finally, introduction of shocks into hodograph design seems useful only in connection with viscous layer interaction. Provided, empirical or computational results of boundary layer displacement exist, including interaction effects from both the shock and the trailing edge, a hodograph solution of a realistic potential outer flow seems possible.

A final step within these first studies is the investigation and comparison of boundary layer computation methods, especially its capability to calculate the displacement thickening behind the shock.

3.4 Comparison with boundary layer computations.

The experimental results for forced transition, discussed in chapter 3.2, were compared with theoretical computations by the method of Nash-Macdonald[4] and Rotta[16], respectively. The measured pressure distribution (Fig. 20) was used as input. Transition was assumed to take place, as in the case of the experiment, at $x/c = 0.15$. Fig. 25 shows that the agreement in displacement thickness and shape factor is good up to the shock; however, both methods overpredict the two parameters due to the pressure rise through the shock. Separation is indicated by both methods, although separation does actually not occur (see Fig. 21a). The program of Rotta stops as soon as separation is indicated, Nash-McDonald continuous downstream and is obviously able to predict the displacement thickness behind the shock quite well. In the range of the rear adverse pressure gradient, however, the disagreement between experiment and theory becomes again fairly large.

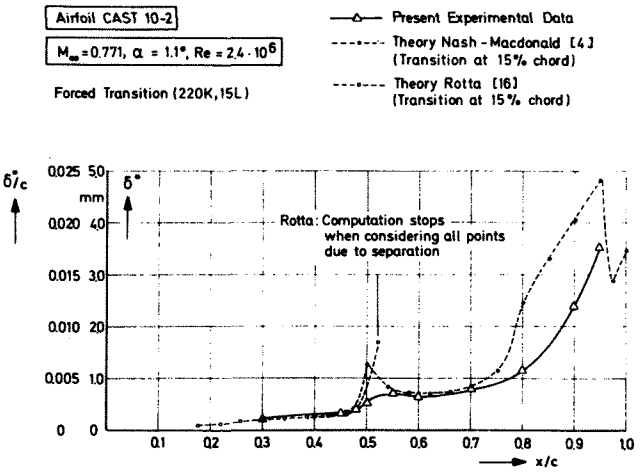

a. Displacement thickness

Figure 25. Comparison of measured and theoretical boundary layer parameters (Input: All points of the pressure distribution)

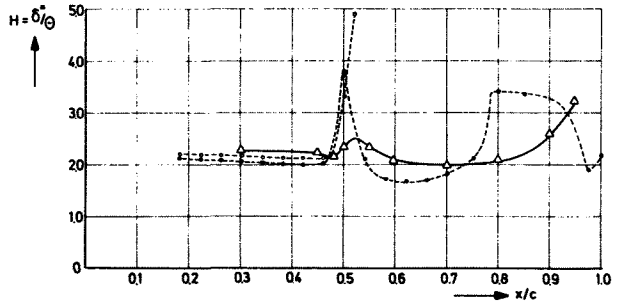

b. Shape factor $H = \delta^*/\Theta$

Figure 25. Concluded

The comparison of the experimental and theoretical data shows that a boundary layer computation method to be used to predict supercritical airfoil flow must properly account for the interaction of the boundary layer with strong adverse pressure gradients. As long as such methods are not available, it seems possible to by pass the problem arising due to the shock, at least up to a certain shock strength, by softening the pressure gradients artificially by omitting critical points in the pressure distribution. This is demonstrated in Fig. 26.

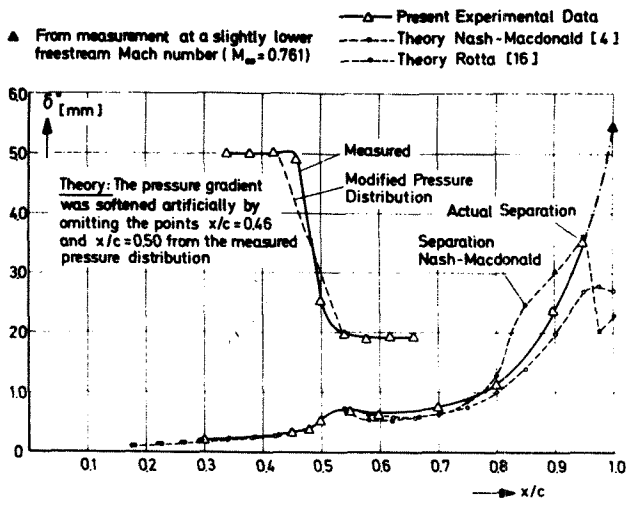

Figure 26. Comparison of measured and theoretical boundary layer parameters (Omission of points at x/c = 0.46 and x/c = 0.50 in the pressure distribution).

4. CONCLUSION

In this paper it was tried to present a combination of theoretical and experimental work on transonic flow for several reasons:

At first it seems necessary to extend hodograph theory of plane inviscid flow to phenomena stemming from interaction with local viscous effects. Shock-boundary layer interference is one of the most drastical examples of such an interaction. Experimental results were used to extend the theory in a realistic way, forming a basis for systematic consideration of viscous effects in inviscid flow design.

The presented experimental results also serve as test cases for the empirical improvement of existing boundary layer computation methods. In consequence, such methods in combination with the inviscid design method should enable the designer to calculate airfoil flows with prescribed shock-boundary layer interaction.

The understanding of transonic scale effects in wind tunnels is another main problem which requires extended experiments in combination with theoretical interpretation. As far as the structure of complicated outer flows is concerned, some answers may be given by potential theory; the structure of viscous layers still leaves many theoretical questions open.

References

1 Sobieczky, H.: Exakte Lösungen der ebenen gasdynamischen Gleichungen in Schallnähe. Z. Flugwiss. 19 (1971), p. 197 - 214

2 Eberle, A.: An exact Hodograph method for the design of supercritical wing sections Symposium Transsonicum II, Göttingen (1975), p. 314 - 321

3. Sobieczky, H.: Entwurf überkritischer Profile mit Hilfe der rheoelektrischen Analogie. DLR-FB 75 - 43 (1975)

4 Bauer, F.; Garabedian, P., Korn, D., Jameson, A.: Supercritical Wing Sections I and II. New York, (1972, 1975).

5 Garabedian, P.: On the design of airfoils having no boundary layer separation. Advances in Mathematics 15, (1975). p. 164 - 168

6 Boerstoel, J.W., Huizing, G.H.: Transonic shock-free aerofoil design by an analytic hodograph method. AIAA paper 74 - 539 (1974)

7 Hicks, R.M., Murman, E.M., Vanderplaats, G.N.: An assessment of airfoil design by numerical optimization. NASA TMX-3092 (1974)

8 Boerstoel, J.W.: Review of the application of hodograph theory to transonic aerofoil design and theoretical and experimental analysis of shock-free aerofoils. Symposium Transsonicum II, Göttingen (1975), p. 109 - 133.

9 Oswatitsch, K., Zierep, J.: Das Problem des senkrechten Stoßes an einer gekrümmten Wand. ZAMM 40 (1960), p. 143 - 144.

10 Ackeret, J., Feldmann, F., Rott, N.: Untersuchungen an Verdichtungsstößen und Grenzschichten in schnell bewegten Gasen. Mitt. Inst. f. Aerodynamik ETH, Nr. 10. Zürich (1946).

11 Sobieczky, H.: Die Struktur der Außenströmung bei transsonischer Stoß-Grenzschicht-interferenz. DFVLR/AVA Report 251-76 A 15 (1976).

12 Stanewsky, E., Zimmer, H.: Entwicklung und Windkanalerprobung von drei überkritischen Profilen für Verkehrsflugzeuge (Development and Wind Tunnel Test of three Supercritical Airfoils for Transport Aircraft) Zeitschrift für Flugwissenschaften 23 (1975), Heft 7/8.

13 Lorenz-Meyer, W.: Test Facilities of the DFVLR in the Transonic and Hypersonic Speed-Range and Main Activities. Deutsche Luft- und Raumfahrt, Forschungsbericht DLR FB 71-86, (1971)

14 Stanewsky, E.: Wall Interference and Scale Effects Encountered in Testing Three Supercritical Airfoils in the DFVLR-AVA 1 x 1 Meter Transonic Tunnel, DFVLR/AVA-Report 251-75 A 38 (1975)

15 Sasman, P.K., Cresci, R.J. . Compressible Turbulent Boundary Layer with Pressure Gradient and Heat Transfer, AIAA Journal, Vol. 4, No. 1, Jan 1966, pp. 19 - 25

16 Rotta, J.-C.: FORTRAN IV - Computer Program for Boundary Layers in Compressible Two-Dimensional and Axisymmetric Flow, Deutsche Luft- und Raumfahrt, Forschungsbericht 71 - 51.